

Empowering human-like walking with a bio-inspired gait controller for an under-actuated torque-driven human model

Amini, Samane; Kardan, Iman; Seth, Ajay; Akbarzadeh, Alireza

DOI

10.1088/1748-3190/adb2ca

Publication date

Document Version Final published version

Published in

Bioinspiration and Biomimetics

Citation (APA)

Amini, S., Kardan, I., Seth, A., & Akbarzadeh, A. (2025). Empowering human-like walking with a bio-inspired gait controller for an under-actuated torque-driven human model. Bioinspiration and Biomimetics, 20(2), Article 026026. https://doi.org/10.1088/1748-3190/adb2ca

Important note

To cite this publication, please use the final published version (if applicable). Please check the document version above.

Copyright

Other than for strictly personal use, it is not permitted to download, forward or distribute the text or part of it, without the consent of the author(s) and/or copyright holder(s), unless the work is under an open content license such as Creative Commons.

Please contact us and provide details if you believe this document breaches copyrights. We will remove access to the work immediately and investigate your claim.

Green Open Access added to TU Delft Institutional Repository 'You share, we take care!' - Taverne project

https://www.openaccess.nl/en/you-share-we-take-care

Otherwise as indicated in the copyright section: the publisher is the copyright holder of this work and the author uses the Dutch legislation to make this work public.



PAPER

Empowering human-like walking with a bioinspired gait controller for an under-actuated torque-driven human model

To cite this article: Samane Amini et al 2025 Bioinspir. Biomim. 20 026026

View the <u>article online</u> for updates and enhancements.

You may also like

- Flapping dynamics and wing flexibility enhance odor detection in blue bottle flies Naeem Haider, Zhipeng Lou, Shih-Jung Hsu et al.
- <u>Using deep reinforcement learning to investigate stretch feedback during swimming of the lamprey</u>
 Oliver Hausdörfer, Astha Gupta, Auke J ljspeert et al.
- A guide to eusocial insect faulted agent resilience and its engineering applications
 James Hand and Bryan Watson

Bioinspiration & Biomimetics



26 August 2024

REVISED

17 November 2024

ACCEPTED FOR PUBLICATION 5 February 2025

PUBLISHED

13 March 2025

PAPER

Empowering human-like walking with a bio-inspired gait controller for an under-actuated torque-driven human model

Samane Amini¹, Iman Kardan¹, Ajay Seth² and Alireza Akbarzadeh^{1,*}

- Center of Advance Rehabilitation and Robotic Research (FUM-CARE), Mechanical Engineering Department Ferdowsi University of Mashhad, Mashhad, Iran
- ² Department of Biomechanical Engineering, Delft University of Technology, Delft, The Netherlands
- * Author to whom any correspondence should be addressed.

E-mail: ali_akbarzadeh_t@yahoo.com

Keywords: human balance control, human gait, torque-driven model, under-actuated human skeletal model, opensim

Abstract

Human gait simulation plays a crucial role in providing insights into various aspects of locomotion, such as diagnosing injuries and impairments, assessing abnormal gait patterns, and developing assistive and rehabilitation technologies. To achieve more realistic gait simulation results, it is essential to use a comprehensive model that accurately replicates the kinematics and kinetics of human movement. Human skeletal models in OpenSim software provide anatomically accurate and anthropomorphic structures, enabling users to create personalized models that accurately replicate individual human behavior. However, these torque-driven models encounter challenges in stabilizing unactuated degree of freedom of pelvis tilt in forward dynamic simulations Adopting a bio-inspired strategy that ensures human balance with a minimized energy expenditure during walking, this paper addresses a gait controller for a torque-driven human skeletal model to achieve stable walking. The proposed controller employs a nonlinear model-based approach to calculate a balance-equivalent control torque and utilizes the hip-ankle strategy to distribute this torque across the lower-limb joints during the stance phase. To optimize the parameters of the trajectory tracking controller and the balance distribution coefficients, we developed a forward dynamic simulation interface established between MATLAB and OpenSim. The simulation results indicated that the torque-driven model achieves a natural gait, with joint torques closely aligning with the experimental data. The robustness of the bio-inspired gait controller was further evaluated by applying a range of external forces on the skeletal model. The robustness analysis demonstrated efficient balance recovery mechanism of the proposed bio-inspired gait controller in response to external disturbances.

1. Introduction

Forward dynamic simulation is a computational method extensively employed in biomechanical systems to precisely replicate human movements [1, 2]. This technique allows the model to closely replicate human behavior, including forces, torques, and motion trajectories [3, 4]. The outcomes of these simulations offer valuable tools for analyzing neuromotor injuries and motor impairment [5]. Thus, employing human locomotion models with the ability to simulate movements closely resembling real human is a crucial role in this field. To perform

forward dynamic simulations of human movements, previous studies have employed various mathematical models of the human body, ranging from conceptual dynamic models to complex multibody dynamic models. For instance, the linear inverted pendulum model and multi-segmental inverted pendulum model are commonly utilized to analyze stability in bipedal locomotion [6–10]. Additionally, complex models featuring multiple lower limb segments and musculoskeletal models with redundant sets of muscle-tendon units have been used to study human behavior accurately [11–13]. Nevertheless, simulation that not only avoids the complexities and computational burdens of complex musculoskeletal models but also possesses the capability to provide accurate simulations of real human motion is of paramount importance.

Torque-driven skeletal human model is a comprehensive model for duplicating human gait, which is not only capable to be scaled according to the anthropomorphic structure of the human body by wearable sensors [14, 15] but also does not have the computational complexities of muscle-based models. In our study, we utilized a skeletal human model equipped with a trunk in the upper body, connected to the lower body by the pelvis joint, and segmented legs including the femur, thigh, and foot, which are connected with the hip, knee, and ankle joints. To derive the dynamic equations of these models, two approaches are commonly employed: fixed-base and floating-base approaches [16, 17]. The fixed-base dynamic approach is frequently utilized to simplify analysis in biomechanics and robotics. It involves breaking down motion into multiple phases or contact states, each corresponding to different configurations of contact points or constraints. For instance, in bipedal locomotion, creating two simplified models for single support and double support phases makes it easier to solve and analyze system dynamics. On the other hand, the floating-base dynamic approach treats the entire bipedal locomotion system as a single entity with a floating-base approach, maintaining the same set of states for every movement.

To ensure realistic results, we derived the dynamic equations of the skeletal human model based on the floating-based approach. This approach helps to avoid discontinuities in joint torques that can occur during transitions between contact states and provides a comprehensive model that covers various movements, which might be overlooked in the fixed-base approach. However, the forward dynamic simulation of a skeletal human model derived from floating-based approach results in an under-actuated model, which leads to mechanically unstable [18]. In fact, the pelvis joint as an unactuated joint is not directly actuated by muscles or external forces in forward dynamic simulation, requiring to maintain balance during walking. Therefore, Our goal in the study is to adopt an appropriate balance control strategy for an under-actuated torque-driven skeletal model that not only replicates the reference human gait but also resembles the kinetic human results with minimal mechanical energy.

Most balance control approaches have been utilized to conceptual or more simple models to simulate human walking without regarding muscle coordination. Zero-moment-point (ZMP) method ensures the static and dynamic stability of the human model by controlling the ZMP to remain within the foot-support region, which is formed

by connecting the foot-ground contact points [19– 21]. In [22], the initial conditions for the stable limit cycle of the passive dynamic model are calculated based on the 'basin of attraction' concept. By setting the initial conditions properly, stable walking cycles can be achieved, closely resembling natural human gait. Moreover, several closed-loop techniques have been proposed to provide robust balance algorithms for bipedal models. These include momentum conservation [23], phase resetting [24, 25], impedance control of joints [26, 27], intermittent control [28, 29], and model-based approaches. Additionally, many studies have been conducted in the field of gait stability approaches based on the concept of human walking. Muscle-reflex controls, which rely on reliance on compliant leg behavior in various subsystems, have been utilized to replicate human walking mechanics and predict the observed activation patterns of some individual muscles [30]. Foot placement control approaches, such as extrapolated COM and capture point concept, ensure stable gait by providing predictions on where to place the foot relative to the body at each step [31]. Neuromuscular models incorporating central pattern generators (CPG) for locomotion control and CPG combined with reflex-based control were proposed to generate rhythmic movements through networks of neural cells [32, 33]. In [34], based on experimental data of subjects recovering to normal walking after facing unforeseen perturbations, a feedback controller was modulated to stabilize a legged model during walking.

In reality, achieving an accurate representation of human gait involves simulating the model in such a manner that either the metabolic cost (in the case of a musculoskeletal model) or the mechanical energy (in the context of a skeletal model) is minimized [35]. In fact, the primary feature of a typical gait, commonly described as efficient or economical, revolves around reducing energy consumption [36]. As humans walk or run, the body has evolved to efficiently utilize energy through different biomechanical methods [37]. Therefore, the aim of this study is to employ a biomechanical perspective in developing a human walking controller that preserves human stabilization with minimal energy expenditure. The hip-ankle strategy is a method of postural control and balance of standing posture that relies on human reactions to external disturbances [38-40]. When standing upright, if a perturbation occurs, individuals may engage their ankle and hip joints, or take a step depending on the magnitude of the disturbance. Researchers in [41] indicated that while all joints contribute to correcting body balance during walking, hip and ankle joints are more involved in the stance phase. Although knee's contribution to the balance of the human body during stance phase

is generally acknowledged, the hip and ankle joints play a more significant role in maintaining balance. Therefore, this study aims to optimize body adjustment using minimal number of joints by focusing on the hip and ankle balance strategies during the stance phase to enable the model to achieve a gait closely resembling the human gait. To simulate and optimize the bio-inspired gait controller, we presented a controllable framework achieved by integrating OpenSim with MATLAB, enabling us to conduct forward dynamic simulation of the skeletal model of OpenSim by scripting controller in MATLAB. This paper is organized as follows: First, gait controller of the under-actuated skeletal model is described. Second, the balance strategy of the gait controller is explained. Next, the optimization process of the bioinspired gait controller is described. Finally, the simulation results of the proposed controller and its performance in response to external disturbance are evaluated in the Results and Discussion section.

2. Methodology

This section elucidates the process of developing a model-based human gait controller to ensure stable walking.

2.1. Gait control of under-actuated torque-driven model

Human torque-driven model is a computational representation of the human body dynamic that focuses on simulating and analyzing human movement driven by joint torques [42]. However, the most critical challenge of the forward dynamic simulation of the torque-driven human model, deriving based on floating-based approach, is the existence of an unactuated degree of freedom (DOF) that needs to employ a balance method. In this section, we utilized an under-actuated torque-driven two-dimensional (2D) model with 9 degrees of freedom to develop a model-based walking controller. Figure 1 represents the under-actuated human model which is used for developing the walking control, and table 1 describes the parameters used in the model. The model includes pelvis joint with one rotational DOF and two degrees of freedom for vertical and horizontal transition. In addition, lower body joints with the hip, knee, and ankle joints have six degrees of freedom. The mathematical model of the model is derived by Lagrange law [41] as follows:

$$\mathbf{M}(\mathbf{q})\ddot{\mathbf{q}} + \mathbf{V}(\mathbf{q},\dot{\mathbf{q}}) + \mathbf{G}(\mathbf{q}) + J_e^T \mathbf{F}_e = \mathbb{T}$$
 (1)

Where, $\mathbf{q} = \begin{bmatrix} \theta_{\text{ankle}}^r, \theta_{\text{knee}}^r, \theta_{\text{hip}}^r, \theta_{\text{ankle}}^l, \theta_{\text{knee}}^l, \theta_{\text{hip}}^l, \\ \theta_{\text{Pelvis}}, X_{\text{Pelvis}} \end{bmatrix}^T \in R^{9 \times 1}$ is the vector of joints variables. $\mathbb{T} = \begin{bmatrix} \mathbb{T}_a \ 0_{3 \times 1} \end{bmatrix}^T \in R^{9 \times 1}$ is the vector of joint torques for actuated joints ($\mathbb{T}_a = \mathbb{T}_a = \mathbb$

 $\tau_a^r, \tau_k^r, \tau_h^r, \tau_a^l, \tau_k^l, \tau_h^l \in R^{6 \times 1})$ and zero torques/forces for pelvis joint, $M(\mathbf{q}) \in R^{9 \times 9}$ is the inertia matrix, $\mathbf{V}(\mathbf{q}, \dot{\mathbf{q}}) \in R^{9 \times 1}$ is the vector of centrifugal and Coriolis forces, $\mathbf{G}(\mathbf{q}) \in R^{9 \times 1}$ is the vector of gravitational forces, $\mathbf{F}_e \in R^{n \times 1}$ is the vector of external force components, $J_e \in R^{n \times 9}$ is a Jacobian matrix relating the position of the applied external forces to the joint variables, and n is the number of external force components, including ground reaction forces. Decomposing actuated and unactuated degrees-of-freedom, equation (1) may be re-written as,

$$\begin{bmatrix} M_{11}(\mathbf{q}) & M_{12}(\mathbf{q}) \\ M_{21}(\mathbf{q}) & M_{22}(\mathbf{q}) \end{bmatrix} \begin{bmatrix} \ddot{\mathbf{q}}_{a} \\ \ddot{\mathbf{q}}_{u} \end{bmatrix} + \begin{bmatrix} \mathbf{V}_{1}(\mathbf{q}, \dot{\mathbf{q}}) \\ \mathbf{V}_{2}(\mathbf{q}, \dot{\mathbf{q}}) \end{bmatrix} + \begin{bmatrix} \mathbf{H}_{1}(\mathbf{q}) \\ \mathbf{H}_{2}(\mathbf{q}) \end{bmatrix} = \begin{bmatrix} \mathbb{T}_{a} \\ 0_{3 \times 1} \end{bmatrix}$$
(2)

where $\mathbf{q}_a = \left[\theta_{\text{ankle}}^r, \theta_{\text{knee}}^r, \theta_{\text{hip}}^r, \theta_{\text{ankle}}^l, \theta_{\text{knee}}^l, \theta_{\text{hip}}^l\right]^T \in R^{6 \times 1}$ is the vector of actuated joints variables, $\mathbf{q}_u = \left[\theta_{\text{Pelvis}}, X_{\text{Pelvis}}, Y_{\text{Pelvis}}\right]^T \in R^{3 \times 1}$ is the vector of unactuated degrees of freedom, and $\mathbf{H}_i(\mathbf{q}) \in R^{n \times 1}\left(H(\mathbf{q}) = G(\mathbf{q}) + J_e^T \mathbf{F}_e\right)$ includes the gravitational and external forces/torques. The actuated and un-actuated dynamic models are derived by dividing the overall system into two subsystems as,

$$M_{11}\left(\mathbf{q}\right)\ddot{\mathbf{q}_{a}}+M_{12}\left(\mathbf{q}\right)\ddot{\mathbf{q}_{u}}+\mathbf{V}_{1}\left(\mathbf{q},\dot{\mathbf{q}}\right)+H_{1}\left(\mathbf{q}\right)=\mathbb{T}_{a}$$

$$M_{21}\left(\mathbf{q}\right)\ddot{\mathbf{q}_{a}}+M_{22}\left(\mathbf{q}\right)\ddot{\mathbf{q}_{u}}+\mathbf{V}_{2}\left(\mathbf{q},\dot{\mathbf{q}}\right)+H_{2}\left(\mathbf{q}\right)=0$$
(3)

Thus, differential equations of two subsystems are obtained as,

$$\begin{bmatrix} \ddot{\mathbf{q}}_{a} \\ \ddot{\mathbf{q}}_{u} \end{bmatrix} = \begin{bmatrix} M_{11}(\mathbf{q}) & M_{12}(\mathbf{q}) \\ M_{21}(\mathbf{q}) & M_{22}(\mathbf{q}) \end{bmatrix}^{-1} \times \left\{ \begin{bmatrix} \mathbb{T}_{a} \\ 0 \end{bmatrix} - \begin{bmatrix} \mathbf{V}_{1}(\mathbf{q},\dot{\mathbf{q}}) \\ \mathbf{V}_{2}(\mathbf{q},\dot{\mathbf{q}}) \end{bmatrix} - \begin{bmatrix} H_{1}(\mathbf{q}) \\ H_{2}(\mathbf{q}) \end{bmatrix} \right\}.$$
(4)

By simeplifying the above equation, we have

$$\ddot{\mathbf{q}}_{a} = M^{*-1}(\mathbf{q}) \left[\mathbb{T}_{a} - \mathbf{V}^{*} \left(\mathbf{q}, \dot{\mathbf{q}} \right) - H^{*}(\mathbf{q}) \right]
\ddot{\mathbf{q}}_{u} = -M_{22}^{-1}(\mathbf{q}) M_{21}(\mathbf{q}) M^{*-1}(\mathbf{q}) \mathbb{T}_{a} - M_{22}^{-1}(\mathbf{q})
\times \left[-\mathbf{V}^{*} \left(\mathbf{q}, \dot{\mathbf{q}} \right) + \mathbf{V}_{2} \left(\mathbf{q}, \dot{\mathbf{q}} \right) - H^{*}(\mathbf{q}) + H(\mathbf{q}) \right]$$
(5)

in which,

$$M^{*}(\mathbf{q}) = M_{11}(\mathbf{q}) - M_{12}(\mathbf{q}) M_{22}^{-1}(\mathbf{q}) M_{21}(\mathbf{q})$$

$$\mathbf{V}^{*}(\mathbf{q}, \dot{\mathbf{q}}) = \mathbf{V}_{1}(\mathbf{q}, \dot{\mathbf{q}}) - M_{12}(\mathbf{q}) M_{22}^{-1}(\mathbf{q}) \mathbf{V}_{2}(\mathbf{q}, \dot{\mathbf{q}})$$

$$H^{*}(\mathbf{q}) = H_{1}(\mathbf{q}) - M_{12}(\mathbf{q}) M_{22}^{-1}(\mathbf{q}) H_{2}(\mathbf{q}).$$

Therefore, the dynamic structure of the underactuated walking model is explained by the differential equation of two actuated and unactuated dynamics (5). As our objective is to control the

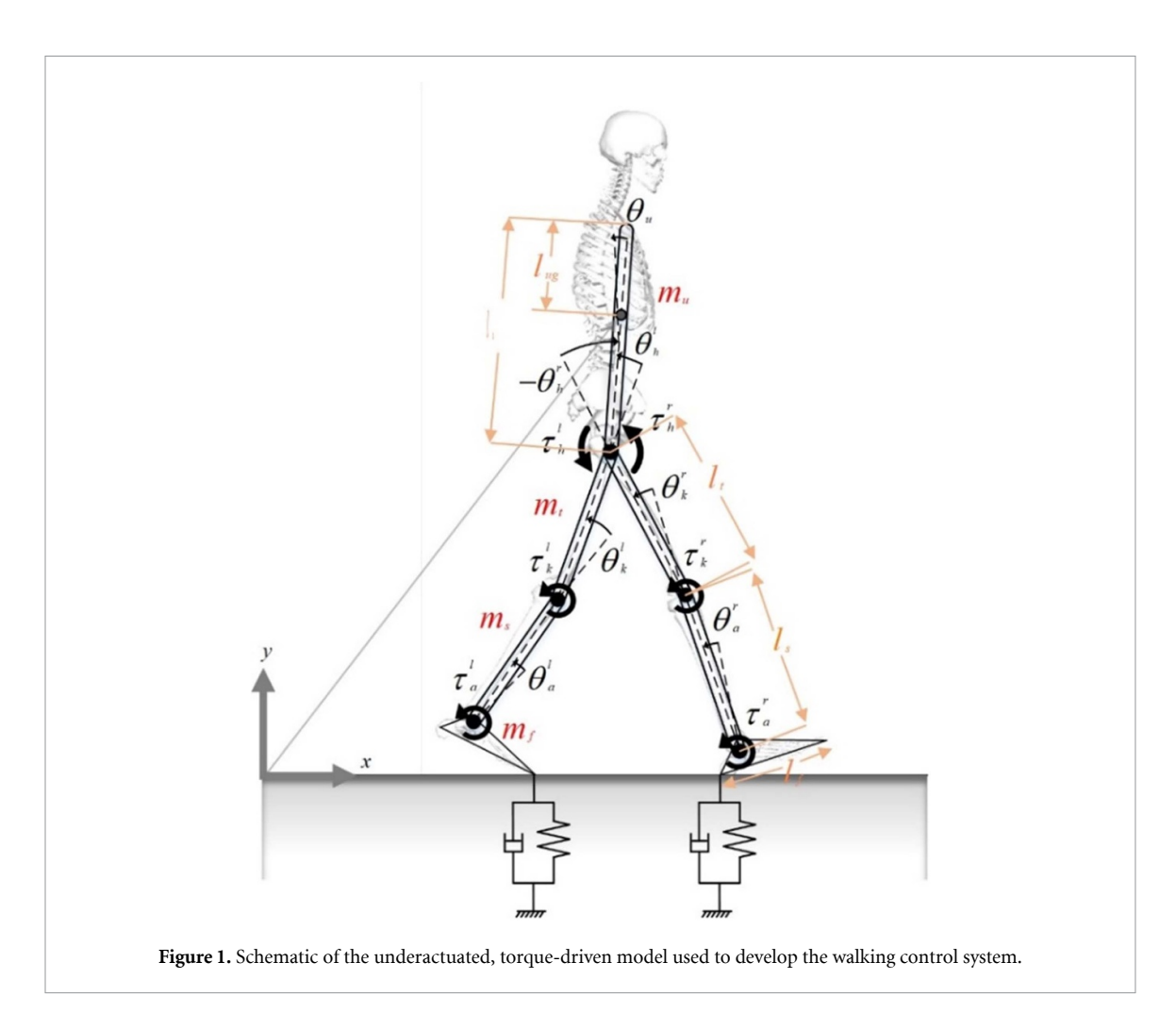


Table 1. Parameters used in the human model.

Symbol	ymbol Description					
(x,y)	<i>x</i> – <i>y</i> positions of central of mass body					
θ_a^r, θ_a^l	Ankle joint angle					
θ_k^r, θ_k^l	Knee joint angle					
θ_h^r, θ_h^l	Hip joint angle					
θ_u^{n}	Pelvis tilt					
$oldsymbol{ au}_a^r, oldsymbol{ au}_a^l$	Ankle torque					
$oldsymbol{ au}_k^r, oldsymbol{ au}_k^l$	Knee torque					
$oldsymbol{ au_h^r}, oldsymbol{ au_h^l}$	Hip torque					
l_t	Length of thigh	0.43 m				
l_s	Length of shank	0.41 m				
l_f	Length of foot	0.18 m				
l_u	Length of upper body	0.78 m				
l_{ug}	Length from COM of upper body to top	0.39 m				
m_t	Mass of thigh	8.25 kg				
m_s	Mass of shank	3.28 kg				
m_f	Mass of foot	1.11 kg				
m_u	Mass of upper body	10.45 kg				

human balance during walking, rather than controlling the position of the model in the sagittal plane, the unactuated dynamic is limited only to pelvis tilt DOF, and control of vertical and horizontal positions of the pelvis is neglected. Therefore the unactuated dynamic is reduced to one DOF ($\ddot{\mathbf{q}}_u \in R^{1 \times 1}$).

Here, we linearize the actuated and unactuated dynamics (5) by defining $\ddot{\mathbf{q}}_a = \mathbf{P}_a$ and $\ddot{\mathbf{q}}_u = \mathbf{P}_u$ as equivalent controls [43]. In this way, the joint torque control becomes:

$$\mathbb{T}_{a} = M^{*}(\mathbf{q}) \mathbf{P}_{a} + \mathbf{V}^{*}(\mathbf{q}, \dot{\mathbf{q}}) + H^{*}(\mathbf{q}).$$
 (6)

The primary objective is for the walking model to accurately follow a specified path trajectory while maintaining stability in the upper body. We utilized a healthy gait dataset as the desired trajectory from [44]. Hence, to track the path trajectory $\mathbf{q}_a^{\text{ref}}$ by the actuated joints \mathbf{q}_a , the equivalent control \mathbf{P}_a is designed as,

$$\mathbf{P}_a = \ddot{\mathbf{q}}_a^{\text{ref}} - \Lambda_d^a \mathbf{e} - \Lambda_p^a \mathbf{e} \tag{7}$$

where $\mathbf{e} = \mathbf{q}_a - \mathbf{q}_a^{\text{ref}}$, $\mathbf{e} = \mathbf{q}_a - \mathbf{q}_a^{\text{ref}}$, $\Lambda_d^a \in R^{6 \times 6}$, $\Lambda_p^a \in R^{6 \times 6}$ are positive diagonal matrices. Furthermore, to ensure the stability of the unactuated subsystem, the equivalent control torque \mathbf{P}_u , is adjusted in accordance with the following equation:

$$\mathbf{P}_{u} = -\Lambda_{d}^{u} \dot{\mathbf{q}}_{u} - \Lambda_{p}^{u} \mathbf{q}_{u} \tag{8}$$

where, $\Lambda_p^u \in R^{1 \times 1}$ and $\Lambda_d^u \in R^{1 \times 1}$ are positive scalars. Ultimately, to achieve stabilization of the overall system, the final equivalent control for the underactuated system is generated by means of a linear combination, expressed as,

$$\mathbf{P} = \mathbf{P}_a + \Pi \, \mathbf{P}_u \tag{9}$$

where $\Pi \in R^{6\times 1}$. represents balance distribution coefficient (BDC), allocated to the actuated joints [45]. By substituting **P** from equation (9) instead of **P**_a in equation (6), the joint torque control for stable walking is computed as described in equation (10).

$$\mathbb{T}_{a} = M^{*}\left(\mathbf{q}\right) \left\{ \left[\ddot{\mathbf{q}}_{a}^{\text{ref}} - \Lambda_{d}^{a} \mathbf{e} - \Lambda_{p}^{a} \mathbf{e} \right] \right\} + \mathbf{V}^{*}\left(\mathbf{q}, \mathbf{q}\right)
+ H^{*}\left(\mathbf{q}\right) + M^{*}\left(\mathbf{q}\right) \Pi\left[-\Lambda_{d}^{u} \mathbf{q}_{u} - \Lambda_{p}^{u} \mathbf{q}_{u} \right].$$
(10)

By simplifying the torque equation, we have:

$$\mathbb{T}_a = \Gamma_a + \Pi \Gamma_u \tag{11}$$

where,

$$\Gamma_{a} = M^{*}\left(\mathbf{q}\right) \left[\ddot{\mathbf{q}}_{a}^{\text{ref}} - \Lambda_{d}^{a}\mathbf{e} - \Lambda_{p}^{a}\mathbf{e}\right] + \mathbf{V}^{*}\left(\mathbf{q}, \mathbf{q}\right) + H^{*}\left(\mathbf{q}\right)$$
(12)

$$\Gamma_{u} = M^{*}(\mathbf{q}) \left[-\Lambda_{d}^{u} \dot{\mathbf{q}}_{u} - \Lambda_{p}^{u} \mathbf{q}_{u} \right]. \tag{13}$$

2.2. Stability analysis

To prove the stability of the walking gait control, we use a positive definite Lyapunov function as follows:

$$V = \frac{1}{2} s^T M^* \left(\mathbf{q} \right) s \tag{14}$$

where $s = \Lambda_d^a \mathbf{e}_a + \Pi \Lambda_d^u \mathbf{q}_u$. The inertial matrix $M^*(\mathbf{q})$ is a positive definite matrix, which implies V > 0 for $s \neq 0$ and V = 0 for s = 0. The derivative of V is given by:

$$\dot{V} = s^T M^* \left(\mathbf{q} \right) \dot{s}. \tag{15}$$

Substituting \dot{s} into \dot{V} , we have:

$$\dot{V} = s^{T} M^{*} \left(\mathbf{q} \right) \left(\Lambda_{d}^{a} \dot{\mathbf{e}}_{a} + \Pi \Lambda_{p}^{u} \dot{\mathbf{e}}_{u} \right). \tag{16}$$

Substituting the equation (10) into equation (16), yields,

$$\dot{V} = s^{T} \left(-\mathbb{T}_{a} + M^{*} \left(\mathbf{q} \right) \ddot{\mathbf{q}}_{a}^{\text{ref}} - M^{*} \left(\mathbf{q} \right) \left[\Lambda_{p}^{a} \mathbf{e} + \Lambda_{p}^{u} \mathbf{q}_{u} \right] + \mathbf{V}^{*} \left(\mathbf{q}, \dot{\mathbf{q}} \right) + H^{*} \left(\mathbf{q} \right) \right). \tag{17}$$

By substituting s, \dot{V} becomes:

$$\dot{V} = \left[\Lambda_{d}^{a} \mathbf{e}_{a} + \Pi \Lambda_{p}^{u} \mathbf{e}_{u}\right]^{T} \left(\mathbb{T}_{a} + M^{*}\left(\mathbf{q}\right) \ddot{\mathbf{q}}_{a}^{\text{ref}} - M^{*}\left(\mathbf{q}\right)\right]$$
$$\left[\Lambda_{p}^{a} \mathbf{e} + \Lambda_{p}^{u} \mathbf{q}_{u}\right] + \mathbf{V}^{*}\left(\mathbf{q}, \dot{\mathbf{q}}\right) + H^{*}\left(\mathbf{q}\right). \tag{18}$$

By simplifying the \dot{V} we have,

$$\dot{V} = -\left[\Lambda_{d}^{a}\mathbf{e}_{a} + \Pi\Lambda_{p}^{u}\mathbf{e}_{u}\right]^{T}M^{*}\left(\mathbf{q}\right)\left[\Lambda_{p}^{a}\mathbf{e} + \Lambda_{p}^{u}\mathbf{q}_{u}\right] + \left[\Lambda_{d}^{a}\mathbf{e}_{a} + \Pi\Lambda_{p}^{u}\mathbf{e}_{u}\right]^{T}\left(-\mathbb{T}_{a} + M^{*}\left(\mathbf{q}\right)\ddot{\mathbf{q}}_{a}^{\text{ref}} + \mathbf{V}^{*}\left(\mathbf{q},\dot{\mathbf{q}}\right) + H^{*}\left(\mathbf{q}\right)\right).$$
(19)

We separate \dot{V} into two terms of first and second $\dot{V} = \dot{V}_1 + \dot{V}_2$. The first term of \dot{V}_1 is shown as follows:

$$\dot{V}_{1} = -\left[\Lambda_{d}^{a}\mathbf{e}_{a} + \Pi\Lambda_{p}^{u}\mathbf{e}_{u}\right]^{T}M^{*}\left(\mathbf{q}\right)\left[\Lambda_{p}^{a}\mathbf{e} + \Lambda_{p}^{u}\mathbf{q}_{u}\right].$$
(20)

Since the $M^*(\mathbf{q})$ is a positive definite matrix, for every $\Lambda_d^a > 0, \Lambda_d^u > 0, \Lambda_p^a > 0$ and $\Lambda_p^u > 0$, we have $\dot{V}_1 \leq 0$. Additionally, \dot{V}_2 is defined as:

$$\dot{V}_{2} = \left[\Lambda_{d}^{a} \mathbf{e}_{a} + \Pi \Lambda_{p}^{u} \mathbf{e}_{u}\right]^{T} \left(-\mathbb{T}_{a} + M^{*}\left(\mathbf{q}\right) \ddot{\mathbf{q}}_{a}^{\text{ref}} + \mathbf{V}^{*}\left(\mathbf{q}, \dot{\mathbf{q}}\right) + H^{*}\left(\mathbf{q}\right)\right). \tag{21}$$

In the above equation, since the reference acceleration $\ddot{\mathbf{q}}_a^{\mathrm{ref}}$ is bounded, we have $M^*\left(\mathbf{q}\right)\ddot{\mathbf{q}}_a^{\mathrm{ref}}<\|\Omega\|$ for some constant $\|\Omega\|$. Another term $\mathbf{V}^*\left(\mathbf{q},\dot{\mathbf{q}}\right)+H^*\left(\mathbf{q}\right)$ represents the gravity and external forces including ground reaction forces applied to the model. As long as the ground reaction forces remain bounded, this term can be bounded, i.e., $\mathbf{V}^*\left(\mathbf{q},\dot{\mathbf{q}}\right)+H^*\left(\mathbf{q}\right)<\|\Psi\|$ for some constant $\|\Psi\|$. Thus, \dot{V}_2 becomes:

$$\dot{V}_{2} \leqslant \left[\Lambda_{d}^{a} \mathbf{e}_{a} + \Pi \Lambda_{p}^{u} \mathbf{e}_{u}\right]^{T} \left(-\mathbb{T}_{a} + \|\Omega\| + \|\Psi\|\right). \tag{22}$$

To guarantee that \mathbb{T}_a compensates for the dynamics of the system, the term $\mathbb{T}_a - (\|\Omega\| + \|\Psi\|)$ must converge to a bounded value. This can be expressed as:

$$\mathbb{T}_a - (\|\Omega\| + \|\Psi\|) = \eta \mathbf{e}_a + \Pi \varsigma \mathbf{e}_u. \tag{23}$$

Where $\eta \in R^{6 \times 6}$ and $\varsigma \in R^{1 \times 1}$ positives matrix, and the right side of the equation is a bounded error. Substituting this into \dot{V}_2 , we get:

$$\dot{V}_{2} \leqslant -\left[\Lambda_{d}^{a} \mathbf{e}_{a} + \Pi \Lambda_{b}^{u} \mathbf{e}_{u}\right]^{T} (\eta \mathbf{e}_{a} + \Pi \varsigma \mathbf{e}_{u}). \tag{24}$$

Thus, \dot{V}_2 is negative, and combining it with \dot{V}_1 , we have $\dot{V} = \dot{V}_1 + \dot{V}_2 \le 0$. This result proves that the walking gait control is stable.

2.3. Bio-inspired balance approach

According to equation (11), the skeletal joint moment comprises both trajectory tracking control and balance control. The first component involves generating joint moments to enable the human model to follow a reference path, while the second component ensures the provision of torques necessary for maintaining balance during walking. Based on our knowledge, human tends to walk with minimum energy expenditure, often referred to as an energy-efficient or economical walking gait [46, 47]. In fact, the human body has evolved to optimize energy usage by employing various biomechanical approaches, such as adjusting walking speed [48], step width [49], and vertical movement of center of mass (CoM) [50].

Hence, we aim to employ a stable walking biomechanical approach to design balance distribution coefficient values that reduce the locomotion energy. To achieve this goal, a method is adopted in which a fewer number of joints are involved in maintaining human balance [51], resulting in the production of less net balance torque and consequently less consumed energy. The hip-ankle strategy, which is a neuromuscular control mechanism employed by humans to maintain balance during standing, is used to preserve balance in mechanical biped models [52]. According to this strategy, when relatively small disturbances affect the CoM, humans tend to employ the ankle strategy. In such cases, ankle torque is utilized to restore the CoM to its desired position and maintain balance. However, when faced with a significantly large disturbance, a torque is applied to the hip joint to generate angular acceleration in the direction of the disturbance. During walking, while all joints contribute to correcting body balance, according to [53] hip and ankle are more involved in stance phase. In this phase, the body adjusts its balance primarily by varying hip and ankle joints in response to disturbance. In [53], it is indicated that applying medial and lateral balance perturbations to the body, balance response strategies involving hip and ankle moments were used to maintain the human balance. Therefore, by introducing inclined pelvis tilt relative to the original state as a destabilizing measure in human balance, we utilized the hip-ankle strategy to maintain balance during walking to correct the balance using a minimal number of joints. To implement this strategy, we defined a piecewise linear function for the Balance Distribution Coefficients(BDC) which are assigned parameters to the hip and ankle joints as follows,

In which ϕ is the gait phase including 'Early-Stance (ES), Mid-Stance (MS), Terminal-Stance (TS), Swing (S)', determined by ground reaction forces of right leg. α represents the coefficients of the hip and ankle for the right and left legs and, no value is assigned to the knee joint. In addition, as the stance leg has a decisive role in maintaining balance of the human body, BDC is only assigned to the stance phase and this quantification in the swing phase is omitted. In equation (14), the sum of the BDC of the right and left sides equals one for each phase of ES, MS, and TS. As the mid-stance of the right leg is the swing phase of the left side, $^{\text{MS}}\alpha_{\text{hip}}^{\text{left}}$ and $^{\text{MS}}\alpha_{\text{ankle}}^{\text{left}}$ equals zero.

2.4. Bio-inspired gait controller optimization

In order to derive the parameters of the gait controller, a forward dynamic simulation and optimization framework is essential. Researchers have developed forward and predictive simulation frameworks capable of optimizing various gait controllers for tracking motion data or generating new trajectories, respectively [54]. These frameworks, equipped with reflex-based controls, work based on muscle coordination. In our study, we presented a forward dynamic simulation of the torque-driven human model using a controllable framework to optimize the controller parameters without directly addressing muscle excitation. Specifically, we established an interface between MATLAB and OpenSim software,

facilitating interaction with the OpenSim API [55] via MATLAB commands. Within the framework, by receiving kinematic feedback from human model and ground reaction forces from OpenSim, the modelbased control generates joint torques to simulate the skeletal human model. To optimize the parameters of the gait controller we used Genetic Algorithm (ga toolbox) in MATLAB in the simulation and optimization framework. Figure 2 displays the configuration of a bio-inspired gait controller within OpenSim and MATLAB framework.

The design variables requiring optimization encompass parameters of the gait controller, including both actuated and unactuated equivalent controls $\Lambda_d^a, \Lambda_p^a, \Lambda_d^u$ and Λ_p^u along with BDC $\alpha_{\rm hip}^{\rm right}$, $\alpha_{\rm ankle}^{\rm right}$, $\alpha_{\rm hip}^{\rm left}$, $\alpha_{\rm ankle}^{\rm left}$. The following equation represents the objective function of the optimization problem, which aims to minimize both the tracking error of the desired trajectory (J_{TE}) and the mechanical energy (J_{ME}) .

$$J = J_{\text{TE}} + J_{\text{ME}}$$

where,

$$J_{\text{TE}} = \sum_{j}^{i} \left(\mathbf{q}_{ij}^{n} - \mathbf{q}_{ij} \right), i = \text{left, right,}$$

$$j = \text{hip, knee, ankle}$$

$$J_{\text{ME}} = E_{\text{MW}}, E_{\text{MW}} = \sum_{j}^{i} E_{j}^{i} + E_{\text{Pelvis}}.$$
(26)

$$I_{\rm ME} = E_{\rm MW}, E_{\rm MW} = \sum_{i}^{i} E_{j}^{i} + E_{\rm Pelvis}.$$
 (27)

In which E_j , and E_{Pelvis} are mechanical energy of lower limb joints and pelvis joint respectively. In the above equation, the mechanical energy is calculated by multiplying joint moment and joint angular velocity. We applied constraints to our optimization problem. The control parameters were bounded by specific upper and lower limits. The BDC were constrained to lie between zero and one $(0 < \alpha < 1)$.

Furthermore, for each phase ES, MD, and TS, the sum of the BDC for both the right and left sides was set to equal one, as follows:

$$\sum_{j}^{i} \alpha_{j}^{i} = 1, i = \text{left}, \text{right}, j = \text{hip}, \text{ ankle}.$$

The optimization was performed on a computer with a 3.60 GHz Intel i5-8350 U processor and 16 GB of RAM. The reported results were obtained using OpenSim release 4.3 and MATLAB release 2021b. Simulation time of a gait cycle is approximately less than 2 min. Moreover, the optimization process of the gait balance control parameters took almost 24 h to complete. The results of optimization are brought in table 2.

3. Results & discussion

Leg6dof9musc.osim model with 66.5 kg mass and 1.66 m height was used to simulate the bio-inspired walking control performance [56]. The model has nine degrees of freedom including lower limb joint angles (hip, knee, and ankle) and upper body (pelvis tilt, vertical and horizontal pelvis coordination). To generate force between feet and ground, three nonlinear Hunt-Crossley contact models on toes and calcn were used. One sphere is located on calcn with 5 cm radius and two on toes with 2.5 cm [54]. Figure 3 displays the optimized BDC as described in equation (9) during the stance phase including Early-Stance (ES), Mid-Stance (MS), and Terminal-Stance (TS). The results are provided for one gait cycle of the right

It is seen that the equivalent torque control (\mathbf{P}_u) undergoes changes during stance phase. During the early-stance, the average of P_u is between -1 Nm kg⁻¹ and 7 Nm kg⁻¹. In this phase, the BDC values for the hip and ankle are 0.17 and 0.08, respectively, indicating more weight is assigned to the hip joint, which confirms the hip strategy. In the mid-stance phase, the average of P_u is between -2.5 Nm kg^{-1} and 3 Nm kg⁻¹, indicating minimal disturbances on the upper body. As expected, there is an increase in the ankle BDC, reaching its maximum value of 0.58. This corresponds to the ankle strategy, where the ankle joint plays a role in maintaining body balance when small disturbances act on the body. The maximum value of P_u changes from -3 N·m kg⁻¹ in the single stance zone to $5 \text{ N} \cdot \text{m kg}^{-1}$ in the opposite direction in the terminalswing phase, leading to significant body instability in this phase. Therefore, a significant increase in hip BDC is generated to overcome the instabilizing disturbances. Based on the alignment of simulation results with the biomechanical hip-ankle strategy, it can be concluded that the torque-driven control model exhibits performance similar to the pattern of real human walking which attempts to maintain human balance. In figure 4, the kinematic and kinetic results of the torque-driven model simulation are compared with a desired human gait dataset [44]. According to the figure, the joint angle patterns predicted by the bio-inspired gait controller closely resemble those observed in humans. Focusing on the hip joint angle of the desired gait, a peak extension moment is observed during the loading response phase, while a peak flexion moment occurs in the preswing phase. The extension moment of the hip joint refers to the rotational force or torque generated when the hip joint moves into extension. This moment is primarily produced by the contraction of the hip extensor muscles, including the gluteus maximus, hamstrings (specifically the biceps femoris muscle),

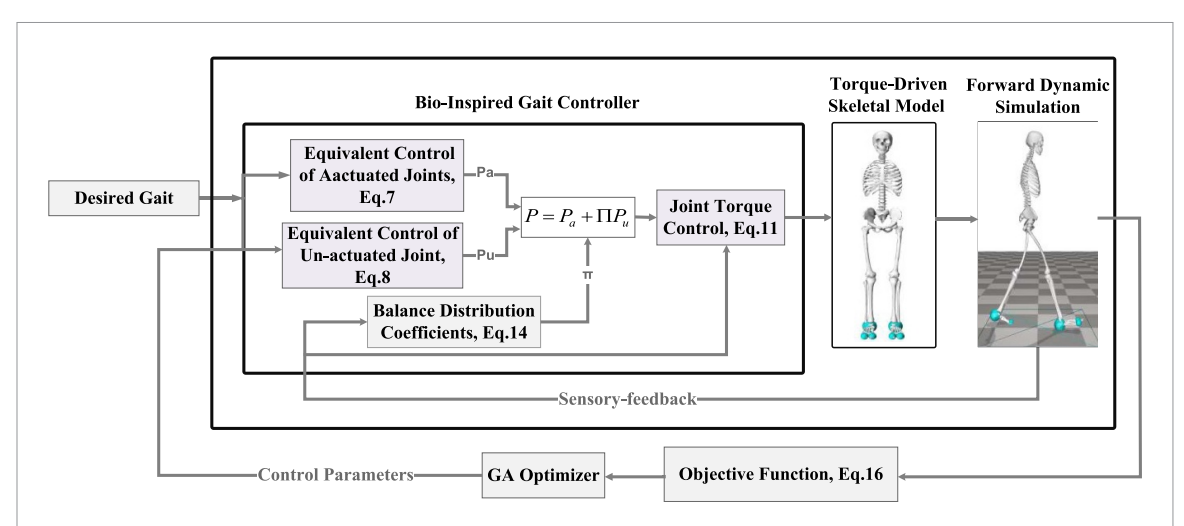


Figure 2. Schematic diagram of the forward dynamic simulation control interface between MATLAB and opensim: the torque-driven skeletal human model is simulated using joint torques generated by a bio-inspired gait control scripted in MATLAB.

Table 2. Parameters of bio-inspired control and objective function values.

Matrix	$\Lambda_{\mathrm{p}}^{\mathrm{a}}$						$\Lambda_{\mathrm{p}}^{\mathrm{a}}$					
Parameter Value	${}^{a}K_{p}^{r}$ 1778.2	${}^{a}K_{p}^{r}$ 1734.0	${}^{h}K_{p}^{r}$ 1012.0	^a K ^l _p 1999.9	^k K ^l _p 1809.3	${}^{h}{ m K}^{l}_{p}$ 1900.0	${}^{a}K_{d}^{r}$ 1532.7	^k K ^r _d 907.0	^h K ^r _d 920.4	${}^{a}K_{d}^{l}$ 1938.0	${}^kK_d^l$ 430.9	${}^{h}K_{d}^{l}$ 203.08
Coefficient	$lpha_{ m hip}^{ m right}$			$lpha_{ m ankle}^{ m right}$			$lpha_{ m hip}^{ m left}$			$lpha_{ m ankle}^{ m left}$		
Parameter Value	ES 0.17	MS 0.44	TS 0.58	ES 0.07	MS 0.56	TS 0.06	ES 0.10	MS 0.56	TS 0.24	ES 0.25	MS 0.44	TS 0.50
Parameter	$\Lambda^u_{ m p}$	$\Lambda^u_{ m d}$										
Value	277.3	1137.3										

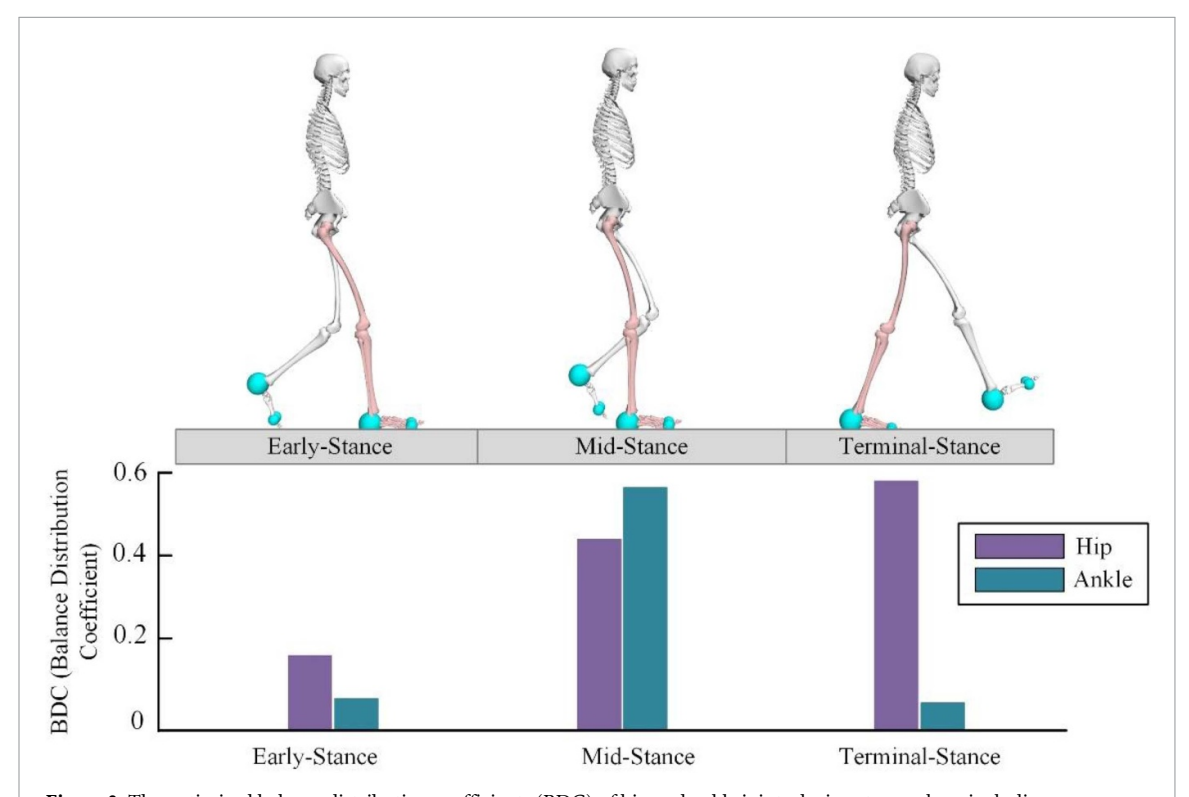


Figure 3. The optimized balance distribution coefficients (BDC) of hip and ankle joints during stance phase including early-stance (ES), Mid-stance (MS), and Terminal-stance (TS). The coefficients belong to the highlighted right leg.

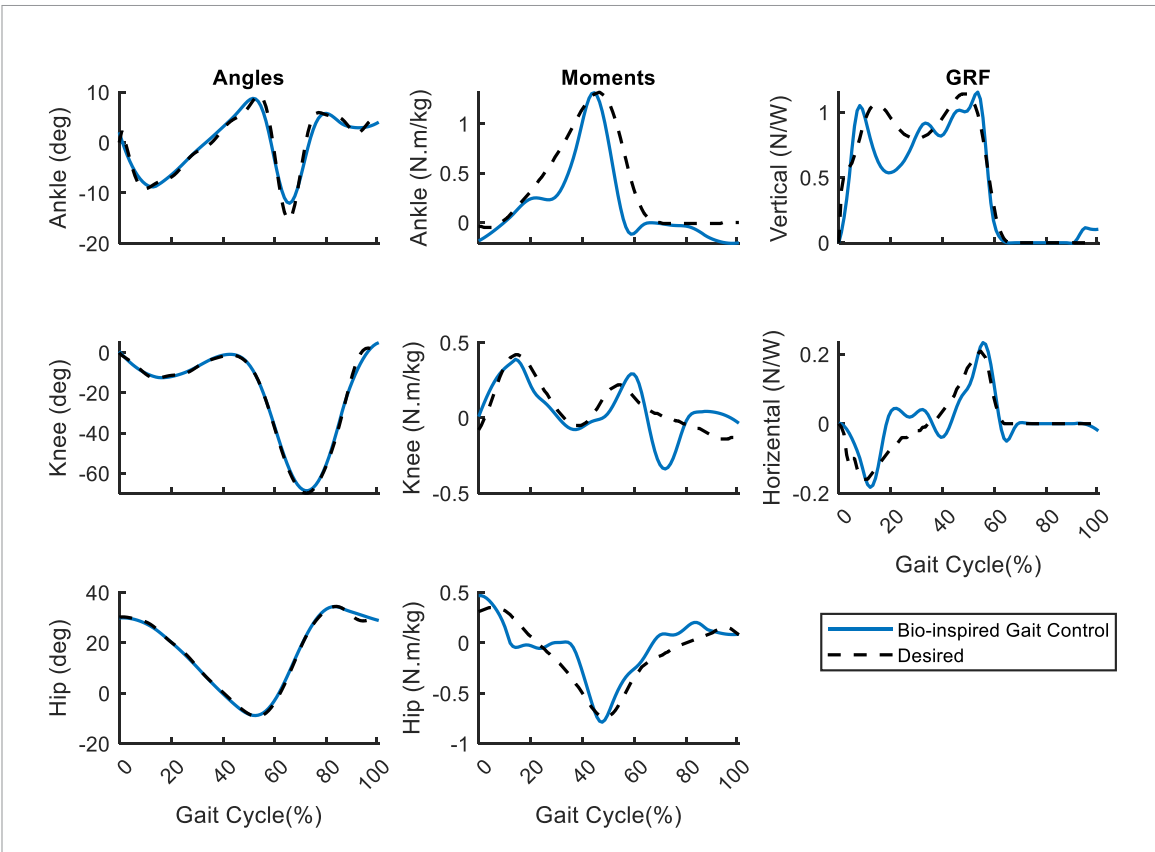


Figure 4. Comparison of joint angles, moments(hip, knee and ankle) and ground reaction forces between the simulated torque-driven model equipped by bio-inspired gait controller and desired gait.

and adductor magnus. On the other hand, the flexion moment of the hip joint is primarily produced by the contraction of the hip flexor muscles, including the iliopsoas (composed of the iliacus and psoas major muscles), rectus femoris, and sartorius muscles. The comparison highlights the behavior of the torquedriven model, which approximately aligns with the desired gait. When comparing knee joint patterns, it is observed that the torque-driven model exhibits flexion during the pre-swing event similar to the desired gait. In the following, a late knee flexion is observed in the swing phase, possibly due to the absence of weight assignment to the knee joint in this model. In terms of the ankle joint, a peak moment is identified in the plantarflexion moment. This moment allows the foot to push off the ground and propel the body forward. It is primarily generated by the contraction of the calf muscles, namely the gastrocnemius and soleus muscles, in the lower leg. The torque-driven model, influenced by the bio-inspired gait controller, effectively replicates this performance.

Overall, this figure demonstrates how both the torque-driven model and human exhibit similar joint moments, providing insights into the functional characteristics and muscle activations during various phases of gait. However, by improving the accuracy of phase detection, we can assign more distributed

weights to the joints, resulting in more reliable simulation results. The ground reaction force plays a crucial role in the study of human gait, providing valuable insights into the mechanics of walking. By comparing the ground reaction forces between the torquedriven model and the human dataset, we see a similar pattern of contact forces. However, there's a significant reduction in vertical force around the middle of stance phase. This reduction is particularly noticeable. The model only used three contact force models, specifically in the toe and heel, and did not include any contact model for the middle of the foot. This absence of modeling resulted in inaccurate ground reaction force compared to the realistic data. Despite the drawback in force modeling, the results indicate that the torque-driven model closely approximates the interaction between the foot and the ground, similar to the observed behavior in actual human subjects.

Table 3 presents the root mean squared error (RMSE) of joint angles, moments, and ground reaction forces of our simulation with the desired gait. It is evident from the table that the RMSE in the hip and knee joint angles is less than 1 degree. However, the ankle angle exhibits an error greater than expected, possibly attributed to the contact force model. By comparing the simulation results for angles,

Table 3. Root mean squared error of bio-inspired gait controller of a torque-driven model.

	Angles (deg)			N	Moments (N	m)	GRFs (N)		
RMSE	Hip	Knee	Ankle	Hip	Knee	Ankle	Vertical	Horizontal	
	0.5115	0.2557	1.0515	0.37	0.24	0.50	0.40	0.16	

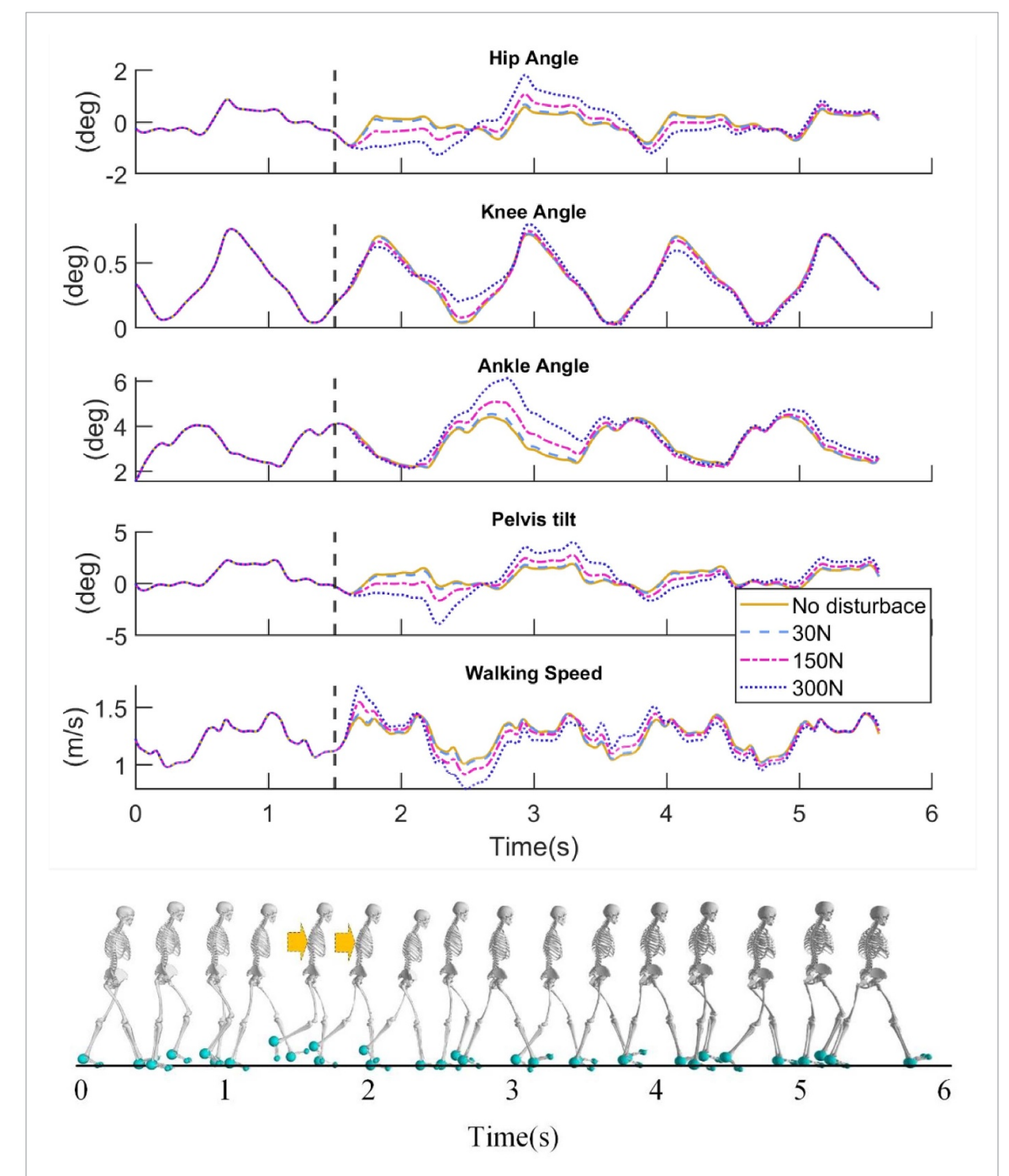


Figure 5. Top:Performance of the torque-driven human model with bio-inspired gait controller against external disurbances. on error tracking of joint angles (hip, knee, and ankle) and pelvis tilt and Gait speed. Dashed line indicates the instance time of applying disturbance. Bottom: Gait pattern of the human skeletal model in response to a 300 N applied disturbance force on the upper body of the model. The highlighted arrow illustrates the disturbance force applied to the human body.

moments, and ground reaction forces, it becomes evident that our controller exhibits a reliable capability in tracking the desired path accurately. In the next simulation, the robustness of the bio-inspired walking control is assessed by subjecting the model's torso to disturbance forces of different amplitudes. These forces included low disturbance (30 N), moderate disturbance (150 N), and large disturbance (300 N) applied horizontally, 20 cm above the center of mass of the torso. Figure 5 illustrates the impact of these

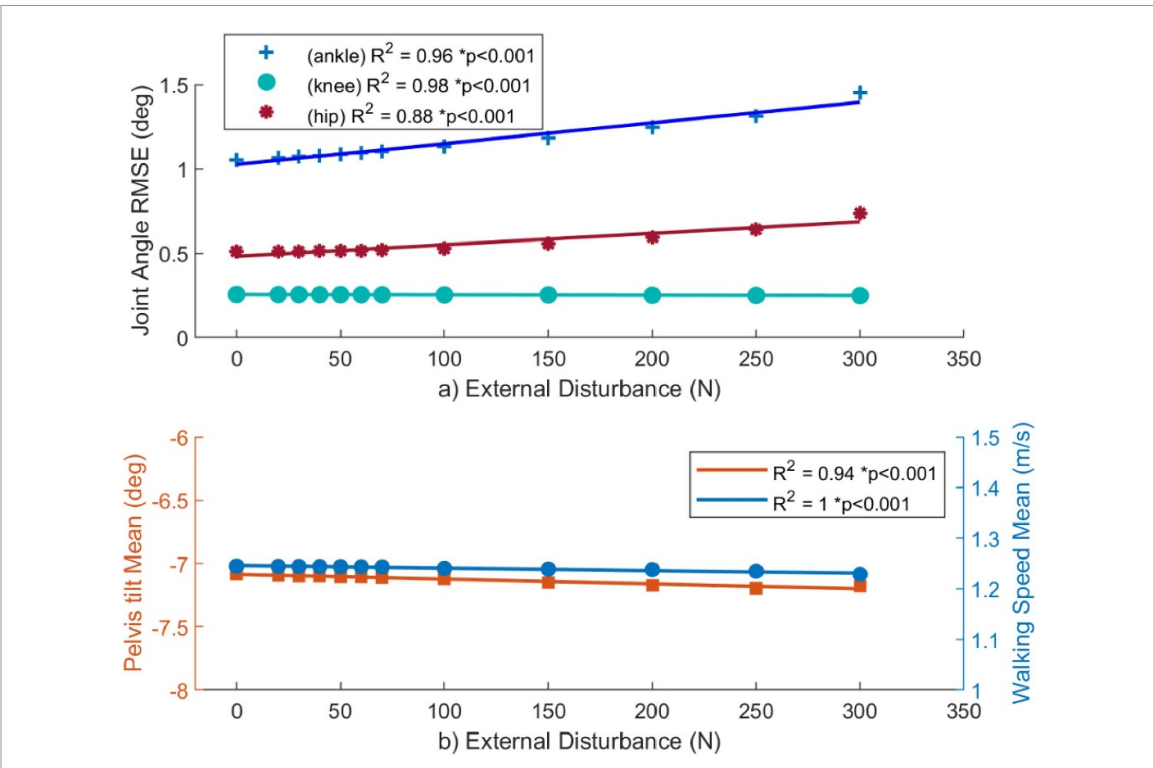


Figure 6.: Correlation of motion kinematics with amplitude of the external disturbance, (a) correlation of root mean square error of torque-driven joint angles with external disturbance, (b) correlation of mean pelvis tilt angle and mean walking speed with external disturbance forces. *P*-value for all results is less than 0.001, calculated at 99.9% confidence level *R*-Squared values are $R^2 = 0.98$, and $R^2 = 0.88$ for ankle, knee, and hip joint angles, and $R^2 = 0.94$ and $R^2 = 1$ for mean pelvis tilt and walking speed, respectively. This demonstrates the goodness of fit of the linear regressions. Increasing slopes of the linear regression for hip and ankle joints indicate relevant correlation of these joints with the external disturbance force. The almost horizontal lines in (b) indicate no correlation between tilt angle and walking speed with external disturbances, indicating the robustness of the balance controller.

external disturbances on the deviations of the joint angles from their reference trajectories and pelvis tilt and walking speed as well. The external forces were applied within the time duration from 1.5 to 1.7 s, as highlighted in the dashed line. In the case of a lowlevel disturbance, we observed slight alterations in the angle error and moments of the hip, knee, and ankle joints. However, as the disturbance level increases, more pronounced changes become evident in the hip and ankle joints. This observation demonstrates that these joints are generally more susceptible to external force disturbances compared to the knee. By applying large disturbance, the alterations in the hip and ankle joints become both more extensive and pronounced. Nevertheless, a significant deviation is seen in the hip angle error, which takes a relatively longer period of time to return to its original state compared to the ankle joint. Furthermore, by observingpelvis tilt deviation and walking speed, we can see that even under the highest disturbance, the model returns to its original path in approximately two seconds. The bottom of the figure demonstrates the gait pattern of the human skeletal model in response to 300 N disturbance force applied on the upper body of the

model. To enhance comprehension, we have graphed the R-squared values for RMSE of joint angles in figure 6(a). Additionally, in figure 6(b), we have plotted the mean Pelvis tilt and mean walking speed versus different values of external forces. Figure 5(a) illustrates a clear linear correlation between joint angle RMSE and the increasing disturbance force. Notably, a relatively significant slope was observed in the RMSE linear fitting for the hip and ankle joints which substantiates the significance of these two joints. This observation validates the efficacy of the hip-ankle strategy. Delving deeper, it is worth noting that the slope of the ankle RMSE is slightly more than that of the hip. In fact, while both joints are more engaged during larger disturbances, the ankle joint assumes a more prominent role when dealing with lower levels of disturbance. Analyzing figure 5(b), the low slope exhibited by the mean value of unactuated data (including both mean pelvis tilt (on the left Y-axis) and mean walking speed (on the right Y-axis), indicates a weak correlation between these variables and external forces. This association highlights the successful performance of the bio-inspired gait controller in maintaining the human balance without affecting the overall characteristics of the motion.

4. Conclusion

In this paper, we introduced a bio-inspired gait controller for a torque-driven skeletal model to achieve stable walking with joint trajectory tracking. Since the model is under-actuated and requires a balance maintenance approach, we extended the hip-ankle strategy from the usual cases of upright standing to the case of walking. First, a balance equivalent control torque is calculated using a model-based approach to keep the upper body in an upright position. Then, this torque is distributed to the hip and ankle joints of both legs, in proportion to some 'Balance Distribution Coefficients'. This strategy was applied during the early-stance, middle-stance, and terminalstance phases. To adjust the controller parameters, we established a closed-loop interface between OpenSim and MATLAB for simulating the forward dynamic model. The optimization results confirmed that the torque-driven skeletal model with the proposed controller, exhibits human-like behavior in intrinsically maintaining upper body stability during a walking gait. For instance, when the average balance equivalent control is low in the single stance phase, the ankle joint coefficient increases to compensate for the instability. Similarly, if the average of equivalent control torque is high, the hip joint acts as a balancer. Furthermore, in terms of joint moments, we observed a similar performance between the hip and ankle joints during the loading response and preswing phases. This similarity further supports the effectiveness of the implemented hip-ankle strategy and its ability to replicate human-like walking characteristics. In addition, to assess the robustness of the controller, we exerted a range of horizontal forces on the torso as external disturbances. The simulation results proved the balance recovery performance of the proposed biomechanical gait controller. Overall, our findings demonstrate that the combination of the bio-inspired gait controller and the joint-space model yields results that closely resemble human gait, particularly in terms of maintaining stability and replicating joint torques during specific gait events. There are limitations in this research. The balance control simulation was considered for a 2D human model in the sagittal plane. By considering a three-dimensional human model, the degrees of freedom would increase, and thus, the balance strategy in the frontal plane should also be taken into account. Utilizing the calibrated foot contact models with the ground provides accurate ground reaction forces, leading to appropriate kinetic results. We limited the control problem to walking on flat ground. A potential future work could be to evaluate the model's walking control functionality and ability to maintain balance on sloped and uneven surfaces.

Data availability statement

The data that support the findings of this study are openly available at the following URL/DOI: https://github.com/MechAmini/BioGaitControl-for-HumanWalking.git.

Funding

The authors did not receive support from any organization for the submitted work.

Conflict of interest

The authors have no relevant financial or non-financial interests to disclose.

Author contributions

Conceptualization: Samane Amini, Iman Kardan, Alireza Akbarzadeh.

Data curation: Samane Amini.

Investigation: Samane Amini, Iman Kardan, Ajay Seth, Alireza Akbarzadeh.

Methodology: Samane Amini, Iman Kardan, Ajay Seth, Alireza Akbarzadeh.

Software: Samane Amini, Iman Kardan, Ajay Seth.

Writing—original draft: Samane Amini.

Writing—review & editing: Samane Amini, Iman Kardan, Ajay Seth.

Ethics approval

This study does not contain any studies with human participants or animals performed by any of the authors.

Consent for publication

The authors give their consent for publication of the work 'Empowering human-like walking with a bio-inspired gait controller for an under-actuated torque-driven human model'.

ORCID iDs

Iman Kardan https://orcid.org/0000-0002-5520-1577

Alireza Akbarzadeh 6 https://orcid.org/0000-0001-8605-8956

References

- Ghafari S A, Meghdari A and Vossoughi G 2009 Forward dynamics simulation of human walking employing an iterative feedback tuning approach *Proc. Inst. Mech. Eng.* I 223 289–97
- [2] Waterval N, Veerkamp K, Geijtenbeek T, Harlaar J, Nollet F, Brehm M A and van der Krogt M M 2021 Validation of forward simulations to predict the effects of bilateral plantarflexor weakness on gait *Gait Posture* 87 33–42
- [3] Sylvester A D, Lautzenheiser S G and Kramer P A 2021 A review of musculoskeletal modelling of human locomotion *Interface Focus* 11 20200060
- [4] Ezati M, Ghannadi B and McPhee J 2019 A review of simulation methods for human movement dynamics with emphasis on gait Multibody Syst. Dyn. 47 265–92
- [5] Falisse A, Serrancolí G, Dembia C L, Gillis J, Jonkers I and De Groote F 2019 Rapid predictive simulations with complex musculoskeletal models suggest that diverse healthy and pathological human gaits can emerge from similar control strategies J. R. Soc. Interface 16 20190402
- [6] Alexander R M 1995 Simple models of human movement *Appl. Mech. Rev.* 48 461–70
- [7] Hemami H and Jaswa V C 1978 On a three-link model of the dynamics of standing up and sitting down *IEEE Trans. Syst. Man Cybern. Syst.* 8 115–20
- [8] Komura T, Nagano A, Leung H and Shinagawa Y 2005 Simulating pathological gait using the enhanced linear inverted pendulum model *IEEE Trans. Biomed. Eng.* 52 1502–13
- [9] Cui D, Peers C, Wang G, Chen Z, Richardson R and Zhou C 2021 Human inspired fall arrest strategy for humanoid robots based on stiffness ellipsoid optimisation *Bioinspir*. *Biomim*. 16 056014
- [10] Bao Y and Yang H-W 2024 A three-dimensional spring-loaded inverted pendulum walking model considering human movement speed and frequency Bioinspir. Biomim. 19 046012
- [11] Liu L, Cooper J L and Ballard D H 2021 Computational modeling: human dynamic model Front. Neurorobot. 15 723428
- [12] Hicks J L, Uchida T K, Seth A, Rajagopal A and Delp S L 2015 Is my model good enough? best practices for verification and validation of musculoskeletal models and simulations of movement J. Biomech. Eng. 137 020905
- [13] Taga G 1995 A model of the neuro-musculo-skeletal system for human locomotion: i. Emergence of basic gait *Biol*. *Cybern*. 73 97–111
- [14] Luis I, Afschrift M, De Groote F and Gutierrez-Farewik E M 2022 Evaluation of musculoskeletal models, scaling methods, and performance criteria for estimating muscle excitations and fiber lengths across walking speeds Front. bioeng. biotechnol. 10 1002731
- [15] Nasr A, Hashemi A and McPhee J 2024 Scalable musculoskeletal model for dynamic simulations of upper body movement *Comput. Methods Biomech. Biomed. Eng.* 27 306–37
- [16] Bouyarmane K and Kheddar A 2012 On the dynamics modeling of free-floating-base articulated mechanisms and applications to humanoid whole-body dynamics and control 2012 12th IEEE-RAS Int. Conf. on Humanoid Robots (Humanoids 2012) (IEEE)
- [17] Khalil W, Boyer F and Morsli F 2017 General dynamic algorithm for floating base tree structure robots with flexible joints and links *Hum. Mov. Sci.* 9 031003
- [18] Gupta S and Kumar A 2017 A brief review of dynamics and control of underactuated biped robots Adv. Robot. 31 607–23
- [19] Park S and Oh J 2019 Real-time continuous ZMP pattern generation of a humanoid robot using an analytic method based on capture point Adv. Robot. 33 33–48
- [20] Liu J and Urbann O 2016 Bipedal walking with dynamic balance that involves three-dimensional upper body motion *Robot. Auton. Syst.* 77 39–54

- [21] Al-Shuka H F, Corves B, Zhu W-H and Vanderborght B 2016 Multi-level control of zero-moment point-based humanoid biped robots: a review *Robotica* 34 2440–66
- [22] Yamasaki T, Nomura T and Sato S 2003 Possible functional roles of phase resetting during walking *Biol. Cybern*. 88 468–96
- [23] Bayon C, Emmens A R, Afschrift M, Van Wouwe T, Keemink A Q, van der Kooij H and van Asseldonk E H 2020 Can momentum-based control predict human balance recovery strategies? *IEEE Trans. Neural Syst. Rehabil. Eng.* 28 2015–24
- [24] Yamasaki T, Nomura T and Sato S 2003 Phase reset and dynamic stability during human gait *Biosystems* 71 221–32
- [25] Tamura D, Aoi S, Funato T, Fujiki S, Senda K and Tsuchiya K 2020 Contribution of phase resetting to adaptive rhythm control in human walking based on the phase response curves of a neuromusculoskeletal model *Front. Neurosci.* 14 464057
- [26] Ugurlu B et al 2015 Variable ankle stiffness improves balance control: experiments on a bipedal exoskeleton IEEE/ASME Trans. Mechatronics 21 79–87
- [27] Lim H-O, Setiawan S A and Takanishi A 2001 Balance and impedance control for biped humanoid robot locomotion Proc. 2001 IEEE/RSJ Int. Conf. on Intelligent Robots and Systems. Expanding the Societal Role of Robotics in the The Next Millennium (Cat. No. 01CH37180) (IEEE)
- [28] Bottaro A, Yasutake Y, Nomura T, Casadio M and Morasso P 2008 Bounded stability of the quiet standing posture: an intermittent control model *Hum. Mov. Sci* 27 473–95
- [29] Gawthrop P, Loram I, Lakie M and Gollee H 2011 Intermittent control: a computational theory of human control *Biol. Cybern.* 104 31–51
- [30] Geyer H and Herr H 2010 A muscle-reflex model that encodes principles of legged mechanics produces human walking dynamics and muscle activities *IEEE Trans. Neural* Syst. Rehabil. Eng. 18 263–73
- [31] Bruijn S M and Van Dieën J H 2018 Control of human gait stability through foot placement J. R. Soc. Interface 15 20170816
- [32] Dzeladini F, Van Den Kieboom J and Ijspeert A 2014 The contribution of a central pattern generator in a reflex-based neuromuscular model Front. Hum. Neurosci. 8 371
- [33] Ryu H X and Kuo A D 2021 An optimality principle for locomotor central pattern generators Sci. Rep. 11 13140
- [34] Joshi V and Srinivasan M 2019 A controller for walking derived from how humans recover from perturbations *J. R. Soc. Interface* **16** 20190027
- [35] Roberts D, Hillstrom H and Kim J H 2016 Instantaneous metabolic cost of walking: joint-space dynamic model with subject-specific heat rate PLoS One 11 e0168070
- [36] Seethapathi N and Srinivasan M 2015 The metabolic cost of changing walking speeds is significant, implies lower optimal speeds for shorter distances, and increases daily energy estimates *Biol. Lett.* 11 20150486
- [37] Schrack J A, Simonsick E M and Ferrucci L 2013 The relationship of the energetic cost of slow walking and peak energy expenditure to gait speed in mid-to-late life Am. J. Phys. Med. Rehabil. 92 28–35
- [38] Morasso P 2022 Integrating ankle and hip strategies for the stabilization of upright standing: an intermittent control model Front. Comput. Neurosci. 16 956932
- [39] Blenkinsop G M, Pain M T and Hiley M J 2017 Balance control strategies during perturbed and unperturbed balance in standing and handstand R. Soc. Open Sci. 4 161018
- [40] Versteeg C S, Ting L H and Allen J L 2016 Hip and ankle responses for reactive balance emerge from varying priorities to reduce effort and kinematic excursion: a simulation study *I. biomech.* 49 3230–7
- [41] Dembia C L, Bianco N A, Falisse A, Hicks J L and Delp S L 2020 Opensim moco: musculoskeletal optimal control *PLoS Comput. Biol.* 16 e1008493

- [42] Wojtyra M 2003 Multibody simulation model of human walking Mech. Based Des. Struct. Mach. 31 357–79
- [43] Lee S-G 2016 Nonlinear feedback control of underactuated mechanical systems Nonlinear Systems-Design, Analysis, Estimation and Control (IntechOpen)
- [44] Bovi G, Rabuffetti M, Mazzoleni P and Ferrarin M 2011 A multiple-task gait analysis approach: kinematic, kinetic and EMG reference data for healthy young and adult subjects *Gait Posture* 33 6–13
- [45] Yeon H, Umemoto K, Shimizu S, Endo T, Matsuno F and Mizuki K 2023 Control system design for a class of non-cascade nonlinear under-actuated systems with an application to a rotary crane system *Mechatronics* 96 103087
- [46] Faraji S, Wu A R and Ijspeert A J 2018 A simple model of mechanical effects to estimate metabolic cost of human walking Sci. Rep. 8 10998
- [47] Koelewijn A D, Heinrich D and van den Bogert A J 2019 Metabolic cost calculations of gait using musculoskeletal energy models, a comparison study *PLoS One* 14 e0222037
- [48] Ralston H J 1958 Energy-speed relation and optimal speed during level walking Internationale Zeitschrift für Angewandte Physiologie Einschliesslich Arbeitsphysiologie 17 277–83
- [49] Maxwell Donelan J, Kram R and Arthur D K 2001 Mechanical and metabolic determinants of the preferred step width in human walking *Proc. R. Soc.* B 268 1985–92

- [50] Ortega J D and Farley C T 2005 Minimizing center of mass vertical movement increases metabolic cost in walking *J. Appl. Physiol.* 99 2099–107
- [51] Aftab Z, Robert T and Wieber P-B 2012 Ankle, hip and stepping strategies for humanoid balance recovery with a single model predictive control scheme 2012 12th IEEE-RAS Int. Conf. on Humanoid Robots (Humanoids 2012) (IEEE)
- [52] Runge C, Shupert C L, Horak F B and Zajac F E 1999 Ankle and hip postural strategies defined by joint torques Gait Posture 10 161–70
- [53] Brough L G and Neptune R R 2024 A comparison of the effects of mediolateral surface and foot placement perturbations on balance control and response strategies during walking *Gait Posture* 108 313–9
- [54] Ong C F, Geijtenbeek T, Hicks J L and Delp S L 2019 Predicting gait adaptations due to ankle plantarflexor muscle weakness and contracture using physics-based musculoskeletal simulations *PLoS Comput. Biol.* 15 e1006993
- [55] Seth A, Sherman M, Reinbolt J A and Delp S L 2011 OpenSim: a musculoskeletal modeling and simulation framework for in silico investigations and exchange *Procedia Iutam* 2 212–32
- [56] Seth A et al 2018 OpenSim: simulating musculoskeletal dynamics and neuromuscular control to study human and animal movement PLoS Comput. Biol. 14 e1006223